Applied Surface Science 344 (2015) 119–127

Contents lists available at ScienceDirect

Applied Surface Science

journal homepage: www.elsevier.com/locate/apsusc

Anti-infection activity of nanostructured titanium percutaneous implants with a postoperative infection model

Jing Tan, Yiting Li, Zhiyuan Liu, Shuxin Qu, Xiong Lu, Jianxin Wang, Ke Duan, Jie Weng, Bo Feng*

Key Laboratory of Advanced Technologies of Materials, Ministry of Education, School of Materials Science and Engineering, Southwest Jiaotong University, Chengdu, Sichuan, China

ARTICLE INFO

Article history:
Received 26 December 2014
Received in revised form 16 March 2015
Accepted 19 March 2015
Available online 25 March 2015

Keywords:
Titania nanotubes
Antibacterial efficiency
Percutaneous implantation
Anti-infection property

ABSTRACT

The titanium percutaneous implants were widely used in clinic; however, they have an increased risk of infection since they breach the skin barrier. Lack of complete skin integration with the implants can cause infection and implant removal. In this work, three titania nanotubes (TNT) with different diameters, 50 nm (TNT-50), 100 nm (TNT-100) and 150 nm (TNT-150) arrays were prepared on titanium surfaces by anodization, pure titanium (pTi) was used as control. Samples were characterized by scanning electron microscopy (SEM), atomic force microscopy (AFM), and contact angle analysis. The antibacterial efficiency of TNT was evaluated in vitro against *Staphylococcus aureus* under the visible light. The results indicated that TNT-100 had the highest antibacterial efficiency under the visible light. Subsequently, TNT implants and pTi implants were placed subcutaneously to the dorsum of New Zealand White rabbits, 10^8 CFU *S. aureus* was inoculated into the implant sites 4 h after surgery. The TNF-alpha and IL-1alpha were determined using enzyme linked immunoassay (ELISA). TNT implants revealed less inflammatory factor release than pTi implants with or without injected *S. aureus* liquid. According to the histological results, the TNT implants displayed excellent tissue integration. Whereas, pTi implants were surrounded with fibrotic capsule, and the skin tissue was almost separated from the implant surface. Therefore, the TNT significantly inhibited the infection risk and enhanced tissue integration of the percutaneous implants compared to pTi. The immersion test in the culture medium suggested that one of causes be probably more proteins adsorbed on TNT than on pTi.

1. Introduction

Infection rates occurring in percutaneous implants increase year by year, including osseointegrated percutaneous prosthetics, bone-anchored hearing aids, dental implants, and ventricular assist devices [1,2]. The severity of infection for percutaneous implants depends in part on the amount of infectious agent present at the interface and time since implantation. Once infection has occurred, there are various pathogens colonizing at the interface which would obstruct the integration between implants and skin. Lack of complete skin integration with the implants permits more pathogens to migrate into the body and colonize, which may cause infection, tissue morbidity, implant removal, and even mortality [3,4]. The poor skin integration with the percutaneous implants can result from epidermal downgrowth, which is marked by the epithelial layer migrating down alongside the implant in an attempt to remove the implant with the ultimate goal of restoring the skin as the defensive barrier [5,6].

Various materials have been reported for percutaneous implants, such as polymers [7–9], tantalum [10], titanium [11,12], ceramics [13], and so on. Among all the materials available, titanium is frequently used in percutaneous applications, because of the good mechanical properties, high corrosion resistance and excellent bicompatibility [14–16]. Meanwhile, there were many strategies targeted at improving the integration between the soft tissue and the percutaneous implants, including surface topography alterations [17,18], protein-coatings [19,20], and antimicrobial modification [21]. Previous work has demonstrated that altering the surface topography by creating micromachined grooves [22], pits [23], or porous surfaces [24,25] can decrease the occurrence of infections and promoted skin-implant integration. However, nanotubular structures have rarely been created on the implant surface for percutaneous applications.

* Corresponding author. Tel.: +86 028 87634023; fax: +86 28 87601371.
E-mail address: fengbo@swjtu.edu.cn (B. Feng).

http://dx.doi.org/10.1016/j.apsusc.2015.03.115
0169-4332/

Table 1
The diameter of samples and main parameters of the anodization.

Sample	Diameter of nanotubes (nm)	Voltage (V)	Treatment time (H)
TNT-50	50	10	1
TNT-100	100	20	1
TNT-150	150	20+25	1+1

Titania nanotubes (TNT) have attracted more and more attention due to their unique topography and controlled dimensions. And the nanotubular structures can be used as the reservoir to store growth factors, antibacterial agents, and so on. Nanotubular-titanium surfaces can improve cellular adhesion and increase cell spreading compared to machine finished surfaces [26]. It has been demonstrated the titania nanotubes have potential for improving cell adhesion and consequently skin attachment [27]. TNTs have potential as photocatalysts and antibacterials, since TNT can respond to UV light and absorb poor visible light. This property is due to the wide band gap of titania [28]. The objective of this work was to evaluate whether TNT was adequate as the barrier to decrease the infection risk when the implants are invasion by bacteria.

In this work, TNT was fabricated on Ti surface by anodization, *Staphylococcus aureus* were chosen to investigate the antibacterial activity of TNT under the visible light. A model of postoperative infection was applied in vivo implant test. The objective of this work is trying to decrease the infection risk of the percutaneous implants and achieve the excellent skin integration.

2. Materials and methods

2.1. Preparation of titania nanotubes (TNT)

Commercially pure titanium disks, 10 mm in diameter and 1 mm thick, were polished by SiC sandpapers and then ultrasonically cleaned with acetone, ethanol, nitric acid/hydrofluoric acid liquor and deionized water sequentially. For use in vivo, titanium bars with 3 mm diameter and 10 mm length were used as implants. Anodization was carried out in a conventional two-electrode configuration at room temperature for 1 h. A titanium disk served as an anode electrode and a high-purity graphite sheet as a cathode electrode with 4 cm separation between them. The electrolyte was a miscible liquid of H_3PO_4 (2 M) and HF (0.15 M). The diameter of nanotubes used for this study and the main parameters of the anodization were shown in Table 1. Afterward, the samples were ultrasonically cleaned with deionized water and then annealed at 450 °C for 3 h in air to achieve anatase-type TNT. Pure titanium (pTi) was used as the control.

2.2. Characterization of samples

The morphology of the TNT and pTi was detected by scanning electron microscopy (SEM, FEI Quanta 200) and atomic force microscopy (AFM, CSPM 5000). The samples were gold-sputtered prior to SEM examination and the 3-dimensional AFM images acquired from an area of 2500 nm × 2500 nm. The wettability of the samples was measured by contact angle analysis.

2.3. Bacteria culture

S. aureus (ATCC 12228) was cultivated in Luria-Bertani (LB medium) at 37 °C in an incubator. The samples were placed on 24-well culture plates and separately incubated in 1 ml of the bacteria-containing medium (10^6 CFU ml^{-1}) under the visible light for different time durations. Before bacteria incubation, the samples were sterilized with UV light overnight.

2.3.1. Antibacterial assay

The viable count of *S. aureus* was evaluated by the MTT assay after 1, 3 and 7 days of culture. The bacteria on the various samples were gently rinsed twice with a sterile phosphate buffered saline solution (PBS) and incubated with a 0.25 mg/ml 3-(4,5-dimethylthiazol-2-yl)-2,5-diphenyltetrazolium bromide (MTT, Sigma) solution at 37 °C for 2 h to allow formazan formation. The formazan was dissolved by dimethyl sulfoxide and the optical density (OD) was determined spectrophotometrically at 570 nm [29,30].

Finally, the antibacterial activity was appraised by the following equation:

$$X\ (\%) = \left(\frac{A-B}{A}\right) \times 100 \quad (1)$$

X indicates the antibacterial ratio, A is the average number of OD value from control sample (the bacterial suspension without any sample in it) and B is the average number of OD value after treatment on given sample.

2.3.2. SEM observation

After bacteria incubation for 7 days, the samples were rinsed three times with PBS, fixed with 2.5% glutaraldehyde at 4 °C for 2 h, and dehydrated sequentially in a series of ethanol solutions for 10 min each. Prior to SEM observation, the samples were dried and gold-sputtered.

2.4. Immersion test in the culture medium

When the implants insert into the body, the surface compositions will rapidly change due to proteins absorbing. So an immersion test was carried out in the culture medium (Dulbecco's modified Eagle medium (DMEM, HyClone) containing 10% fetal bovine serum (HyClone)). After being immersed in the medium for 1 day at 37 °C, the samples were removed, rinsed twice with deionised water and dried. X-ray photoelectron spectroscopy (XPS, Kratos XSAM-800, Al Kα radiation) was used for detecting surface chemistry of the samples before and after immersion. The binding energies were calibrated based on the C1s peak at 248.8 eV corresponding to C-H. The following four samples were investigated in XPS analysis: (1) pTi, (2) TNT, (3) pTi immersed in culture medium (pTi + DMEM), (4) TNT immersed in culture medium (TNT + DMEM).

2.5. Percutaneous implant

Titania nanotubes (TNT) with 100 nm in diameter were prepared on surfaces of titanium bars, and pure titanium (pTi) was used as the control. Nine New Zealand White Rabbits (aged 5–30 months, weight 6–9 kg) were randomly assigned to three groups. Samples were surgically implanted to the animal dorsum. Each animal received the four implants as shown in Fig. 1. After being monitored for 1 week to ensure their health, the rabbits were anesthetized by an intravenous injection of 3% pentobarbital sodium with a dose of 1 ml/kg body weight, and their backs were close-shaved. Thereafter, two subcutaneous pockets were created on each side of the spine. One implant was placed in each pocket leaving approximately 3–5 mm of implant exposed. After 4 h following surgery, these animals received bacterial inoculations (*S. aureus* liquid, 10^8 CFU ml^{-1}) directly to the skin/implant interface in the pockets.

The rabbits were sacrificed with overdose of pentobarbital sodium at 2, 4 and 8 weeks after surgery. Each implant with attached soft tissue was carefully harvested from the animal. The

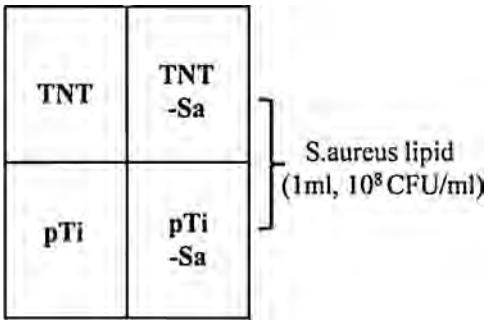

Fig. 1. Overview of the experimental design.

samples were fixed in 10% formalin, dehydrated in serial concentrations of ethanol (70, 80, 90, and 100%), and embedded in methyl methacrylate. Once polymerized, both the transverse section and longitudinal section encompassing the entire implant with surrounding soft tissue was cut with a diamond band saw (Leica 1600, Germany). These sections were then ground using grinding wheel to ~10 μm thick sections and polished. The sections were stained with Van Gieson (VG). Meanwhile, the soft tissues around the implant were formalin-fixed and paraffin-embedded. The sections with a thickness of 5 μm were stained with routine hematoxylin and eosin (H&E). All the sections were observed with a light microscope.

The inflammatory factors (TNF-alpha and IL-1alpha) were determined using an enzyme linked immunoassay (ELISA). The tissues around implants were rinsed with PBS firstly to remove excess blood. And then the tissues were weighed and homogenized in PBS with a glass homogenizer on ice. To further break the cells, the homogenates were splitting with 1% Triton X-100 for 6 h, then centrifuged for 5 min at 5000 × *g* to get the supernate. The TNF-alpha and IL-1alpha concentration of the collected solution was determined using a rabbit TNF-alpha and IL-1alpha ELISA Kit (R&D) respectively. The assay ranges for TNF-alpha and IL-1alpha were 15–1000 pg/ml and 1–250 pg/ml, respectively.

2.6. Statistical analysis

Statistical analysis was performed using one-way analysis of variables (ANOVA) followed by an *F*-test to evaluate differences between groups. $p < 0.05$ was considered statistically significant.

3. Results

3.1. Surface characterization

Fig. 2 shows the surface morphologies of pTi (a), TNT-50 (b), TNT-100 (c) and TNT-150 (d). The sample surface roughness (Ra) obtained by AFM is shown in Fig. 3. Ra depends on the size of the nanotubes and follows the order: TNT-150 > TNT-100 > TNT-50 > pTi. The TNTs surfaces were superhydrophilic since they had contact angles of 0° for water, while pTi surface had 42.9°.

3.2. Antibacterial activity

Fig. 4 shows the antibacterial activity of the samples against *S. aureus* under the visible light. pTi remained a low antibacterial ratio, about 15% during test period, TNTs had an increasing antibacterial

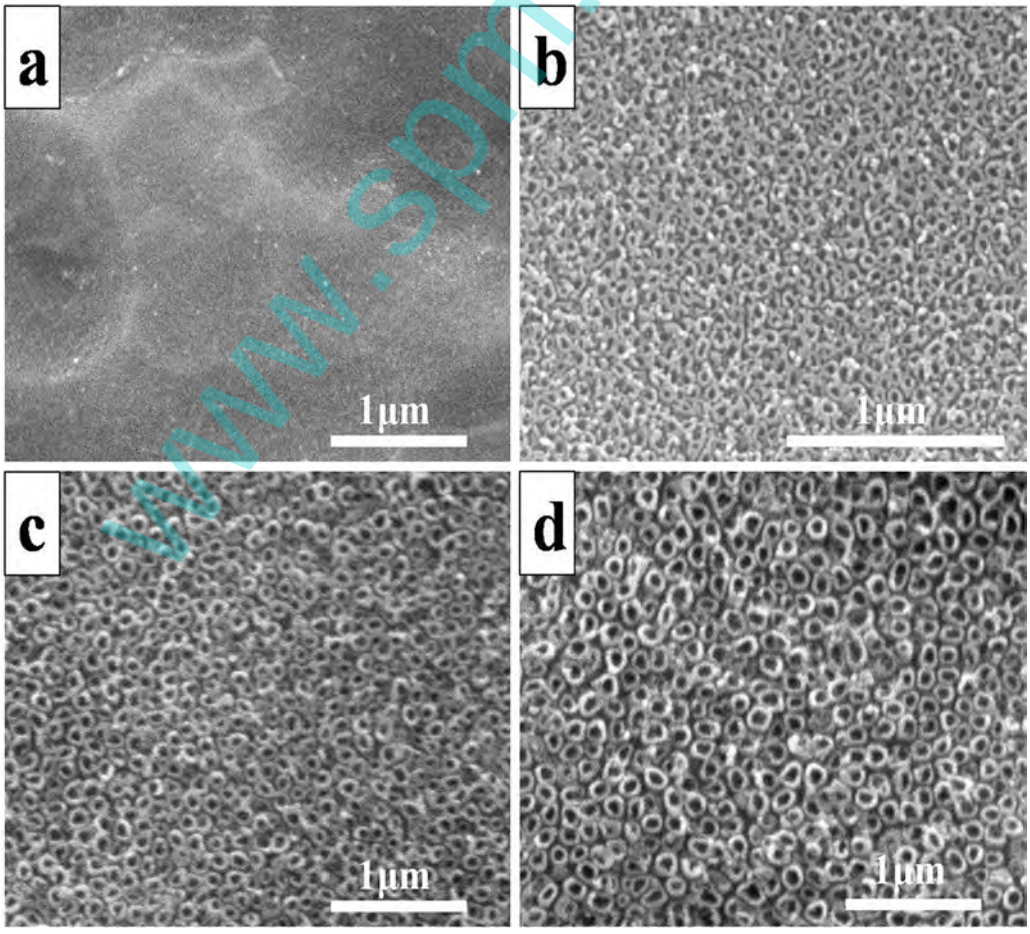

Fig. 2. SEM images of (a) pTi, (b) TNT-50, (c) TNT-100 and (d) TNT-150.

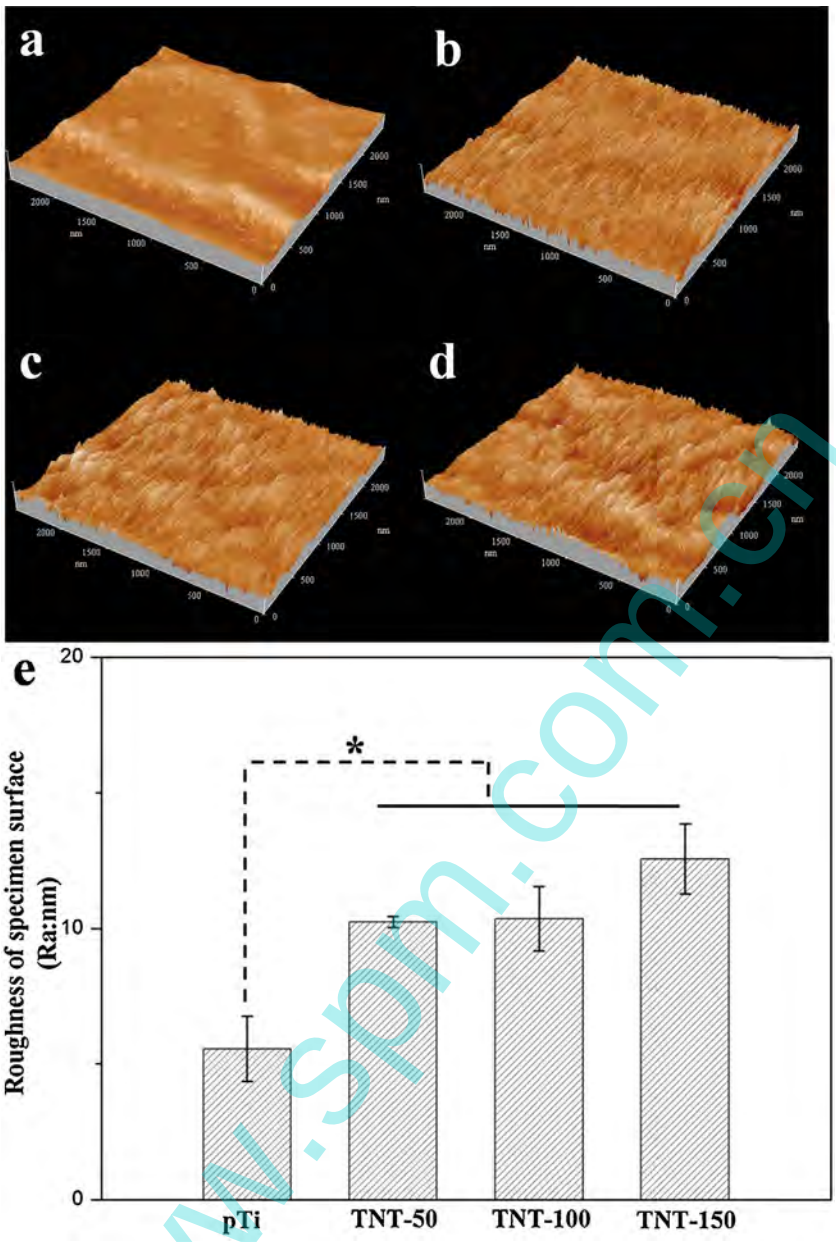

Fig. 3. AFM scans in 3D view over a 2500 nm × 2500 nm region: (a) pTi, (b) TNT-50, (c) TNT-100 and (d) TNT-150. (e) Surface roughness of the various samples determined by AFM.

activity with time lengthening. After culturing for 3 days, the TNT samples showed much higher antibacterial ratio than pTi though after 1 day the ratio of the formers was slightly higher than that of the latter. And TNT-100 sample exhibited the highest antibacterial activity after 7 days, the antibacterial efficiencies was about 70%.

The SEM morphologies of the adherent *S. aureus* after 7 day were shown in Fig. 5. Fewer bacteria were distributed on TNT-100 surface (Fig. 5c) than on the other three samples. The amount of bacteria attached on the flat surface was higher those on nanotubular structured surfaces.

3.3. Protein adsorption in the culture medium

Fig. 6 shows the XPS overview spectra of sample surfaces immersed in DMEM. The N1s peaks revealed the presence of proteins from the culture medium, and the signal intensity was weaker for the pTi + DMEM than for the TNT + DMEM. The Ti2p regions were detected on pTi and TNTs, but not on pTi + DMEM and TNT + DMEM. It indicated that the proteins in the medium have been adsorbed on Ti + DMEM and TNT + DMEM.

The high-resolution spectra of C1s, O1s and N1s were displayed in Fig. 7. After immersion, the peak amine (C-NH_2) (285.5 eV) and peptide bond (O=C—N, 287.5 eV) of C1s can be associated to the typical functional groups borne in the protein on pTi–DMEM and TNT–DMEM. The O1s peak around 532.1 eV can be attributed to the amide functions (O=C—N) of protein, and the peak located at 533 eV was associated to the presence of carbonyl groups (C=O) in several amino acids. The N1s signals were deconvoluted into two peaks at 399.6 eV (O=C—N) and 400.5 eV (C-NH_2). The atomic percentage of the N component was 4.69% and 13.62% for pTi–DMEM and TNT–DMEM respectively. These results further demonstrated that TNT was more available for proteins absorption than pTi. For O1s spectra of pTi and TNT, the major contribution in the XPS curve of pTi came from TiO_2 at a binding energy of 529.9 eV (Ti—O).

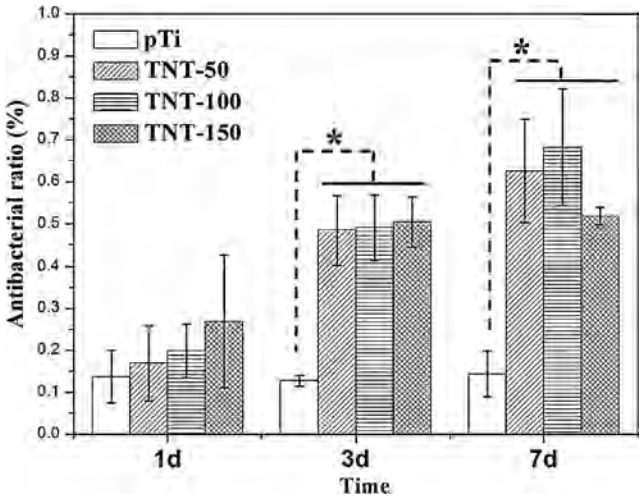

Fig. 4. The antibacterial efficiency of TNT compared with pTi under the visible light against *S. aureus* after 1, 3, 7 days. The data are expressed as means ± standard deviations ($n = 4$).

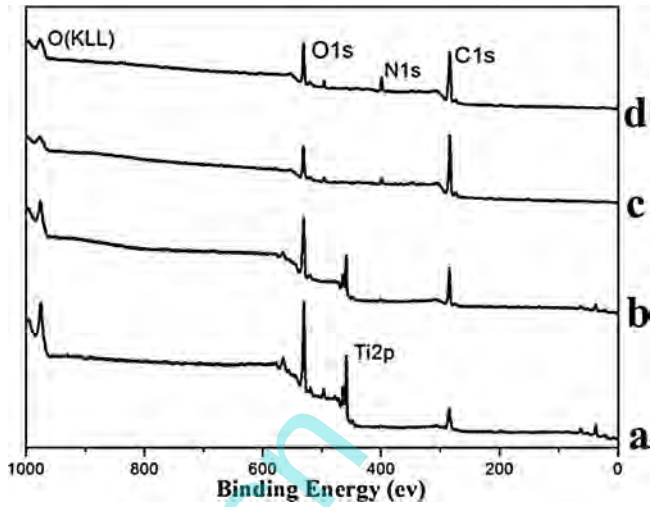

Fig. 6. XPS overview spectra of samples. (a) pTi, (b) TNT, (c) pTi + DMEM, (d) TNT + DMEM.

It was observed that acidic hydroxyl groups $OH_{(a)}$ (530.8 eV) and basic hydroxyl groups $OH_{(b)}$ (532.1 eV) in TNT. The disappearance of Ti—O and OH signals in the pTi–DMEM and TNT–DMEM samples confirmed that proteins have already absorbed onto the samples.

3.4. In vivo evaluation

During the two-week post-operative period, no clinical signs of inflammation were observed at implant sites with injected *S. aureus* lipid, however, the fester appeared around the wound of pTi implant, as showed in Fig. 8. Percutaneous implants may elicit inflammatory responses in adjacent tissues, so the cytokines TNF-alpha and IL-1alpha were detected in exudates from tissues. The values of cytokine for each sample at 2 weeks are provided in Fig. 9. The pTi implant injected *S. aureus* liquid (pTi-Sa) released the highest amount of TNF-alpha and IL-1alpha, whereas TNT had the lowest value. pTi with or without injected *S. aureus* liquid revealed almost the same release of TNF-alpha. The release of IL-1alpha followed the order: pTi-Sa > TNT-Sa > pTi > TNT. The release

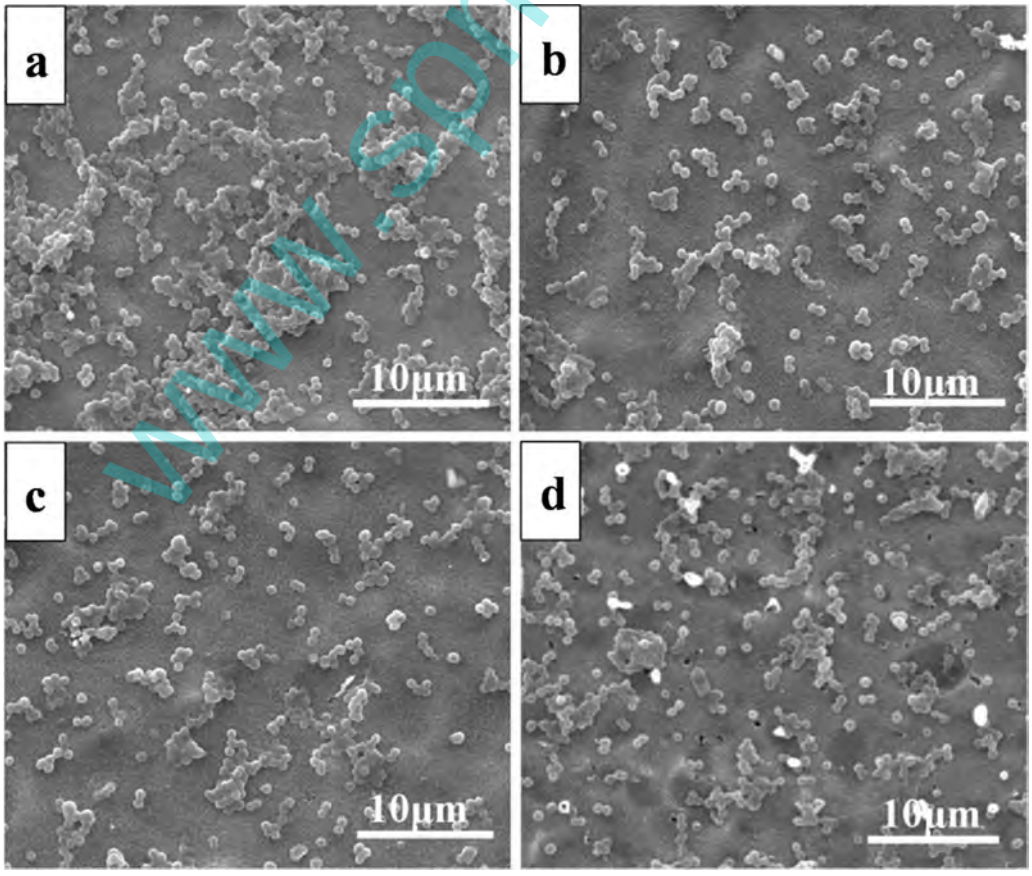

Fig. 5. SEM microphotographs of *S. aureus* after culturing on (a) pTi, (b) TNT-50, (c) TNT-100 and (d) TNT-150 for 7 day.

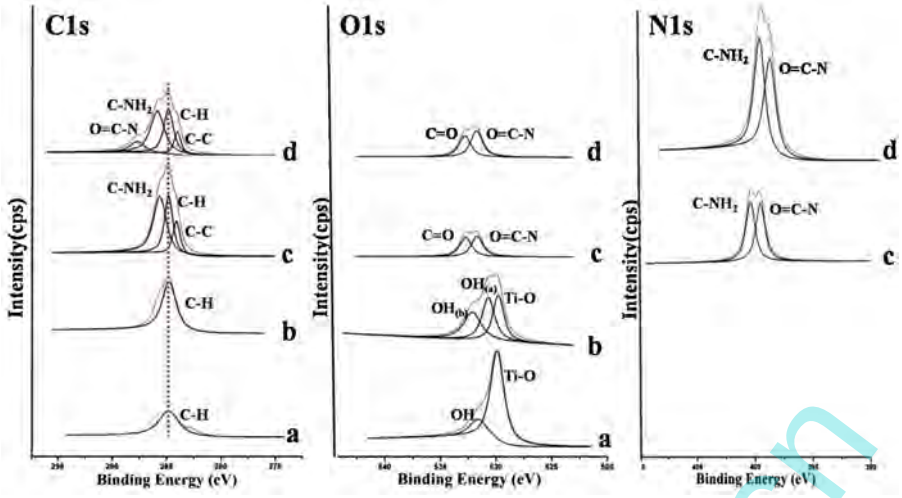

Fig. 7. High-resolution XPS spectra of C1s, O1s and N1s. (a) pTi, (b) TNT, (c) pTi + DMEM, (d) TNT + DMEM.

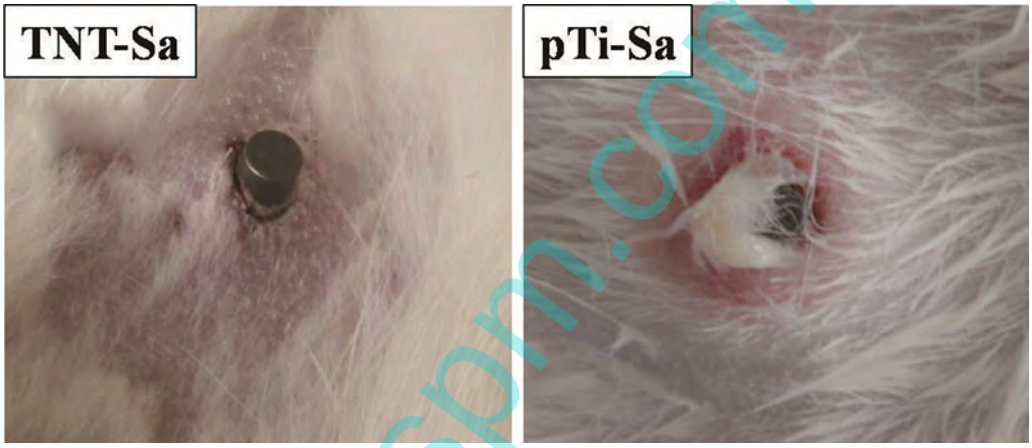

Fig. 8. Implants embedded in back of rabbit after 2 weeks.

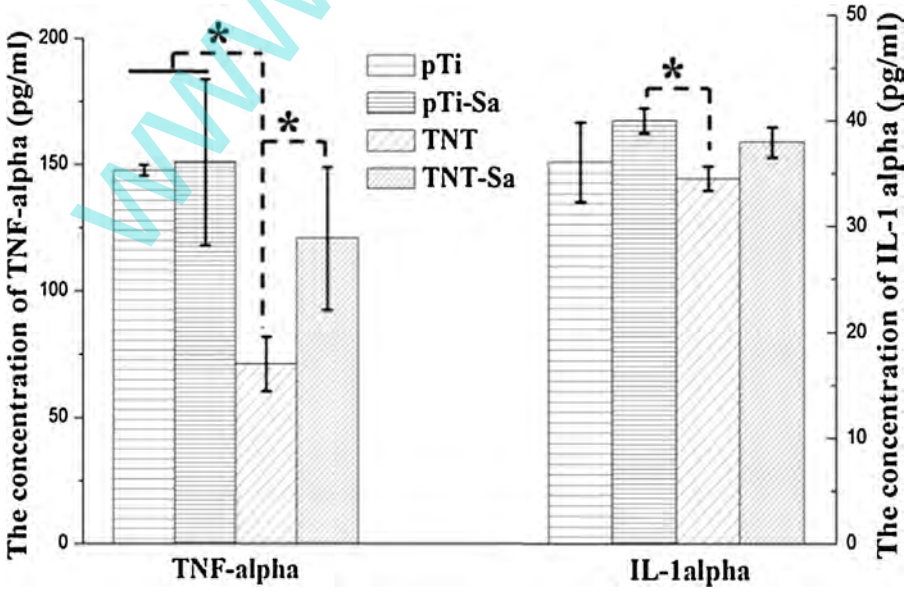

Fig. 9. TNF-alpha and IL1-alpha concentration in pg/mL after 2 weeks of TNT and pTi implant in vivo.

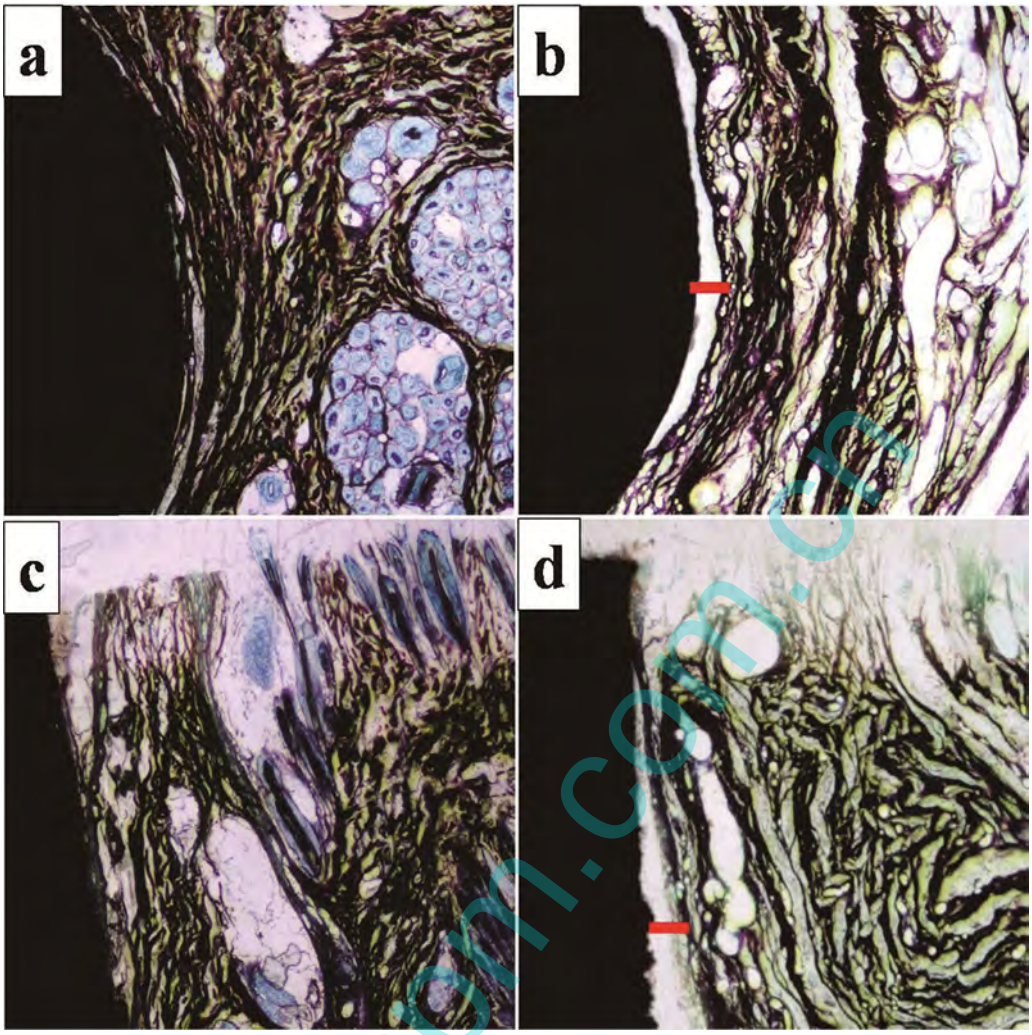

Fig. 10. Light micrographs of Van Gieson staining of the transverse section of the implants with surrounding tissues (a and b) and the longitudinal section of the implants with surrounding tissues (c and d) after 4 weeks. a and c – TNT-Sa; b and d – pTi-Sa; 40×.

of cytokine revealed that TNT had less inflammatory factor production than pTi with or without injected *S. aureus* liquid

Fig. 10a and b shows the transverse sections of the implants with surrounding tissues by Van Gieson staining, which are identical with that of longitudinal section (Fig. 10c and d). The skin tightly adhered to the TNT (Fig. 10a and c), but skin integration with the pTi was poor (Fig. 10b and d). This is strong evidence that the nanostructured surface can improve the cellular and tissue adhesion than pTi. Meanwhile, implants injected bacteria lipid elicited inflammatory responses in adjacent tissues leading to the formation of fibrotic capsules. The fibrotic capsule (Fig. 11, ▲) elicited by TNT was significantly thinner than that induced by pTi. The reactive capsules contained some anti-inflammatory cells such as macrophages, and the TNT implants revealed abundant

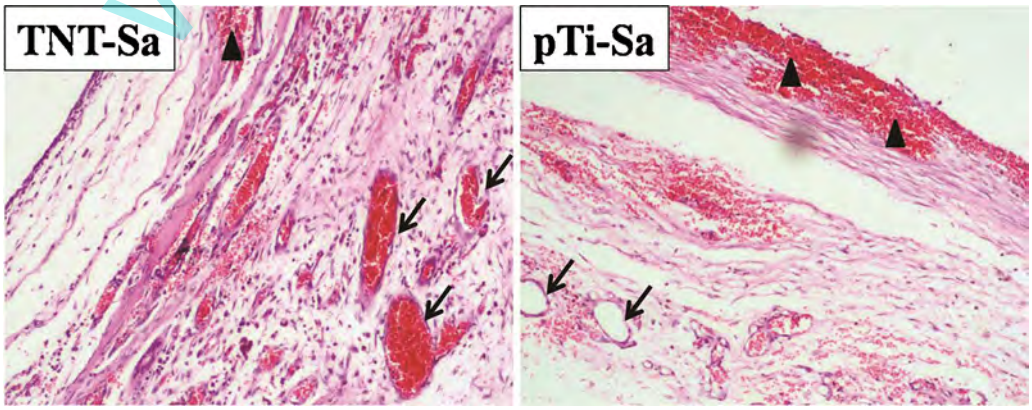

Fig. 11. Light micrographs of hematoxylin and eosin stained the soft tissues around the implants after 4 weeks (100×,: ▲fibrotic capsules, ↙: blood vessel).

anti-inflammatory cells (Fig. 11 staining purple) and blood vessel (↙). In contrast, there are rare anti-inflammatory cells and blood vessels recruited by pTi. As shown by staining results, TNT was much more acceptable than pTi as percutaneous implants, and TNT revealed admirable anti-infection property in the model of postoperative infection.

4. Discussion

Although titanium is non-antibacterial inherently, nanostructured titanium surfaces possess good anti-bacterial property under the UV light and also exhibit weak anti-bacterial ability under the visible light. The photocatalytic antibacterial activity of hierarchical TiO_2 nanorod spheres under the visible light depended on the calcinations temperature [28]. The diameter of nanotubes on titanium surfaces had a direct influence on the utilization efficiency of light which can be attributed to the effect of their specific surface area [31]. In this work, the sample of TNT-100 showed the best antibacterial property under the visible light.

There were many factors related to the interaction between biomaterials and the tissue, such as the surface morphology, wettability and compositions. The surface roughness of TNT was higher than pTi (Fig. 3), the optimal roughness was in favor of cell adhesion. Furthermore, the contact angle test indicated that the wettability of TNT was higher than that of pure Ti disk; this is beneficial to sufficient contact of cells with samples. Thus the nanotubular structure may provide a favorable surface for the growth and maintenance of skin tissue. This will likely translate into an implant interface that allows increased cellular adhesion and enhanced matrix deposition by fibroblasts [32].

Gristina used “race for the surface” to describe the competition between bacterial adhesion and tissue integration [33]. When an implant is inserted into the body, water molecules bind to the surface firstly. Then, a monolayer of protein is rapidly adsorbed which mediate the subsequent cellular adhesion [34]. The XPS analysis suggests that proteins rapidly absorb onto the implant surfaces as immersed in the culture medium (Fig. 6). Judging from O1s spectra of pTi and TNT (Fig. 7 O1s a and b), the nanotubular structure can attract more proteins in biological environment because of the presence of abundant $OH_{(a)}$ and $OH_{(b)}$ groups on TNT surfaces. That is, titania nanotube layers have more OH groups and higher specific surface area, so that can absorb more proteins. Protein absorption on surfaces will affect the integration between implants and tissues. Naturally, when the tissues preferentially adhered to surfaces, bacteria will difficultly attach to the surfaces. Inhibition of bacterial adhesion is often regarded as the most critical step to prevent implant-associated infection.

The skin integration with implants in turn affects the infection rate. With regard to percutaneous implants, tightly and healthy integration with these soft tissues is desirable since the transcutaneous parts face both epithelial and fibrous tissues.

In this work, we design a postoperative infection model to verify that TNT implants can reduce the incidence of infection. During surgery, bacteria adhered to implants will stimulate macrophage to release cytokines. The proinflammatory cytokines, such as TNF-alpha and IL-1alpha, induce the inflammatory cells to migrate to the site of implantation and cause inflammatory responses. Meanwhile, the body initiates a series of wound healing mechanism including inflammatory responses to eradicate pathogen and recover the surrounding tissue. According to the Elisa assay, TNT implants revealed less inflammatory factor release than pTi implants with or without injected *S. aureus* liquid. The intensity of inflammatory responses influences the wound healing, as the migration and aggregation of inflammatory cells may damage cutaneous tissue and cause implantation failure. The absence of soft tissue attachment to the pTi implants was seen during the histological processing as the tissue separated from the implant; whereas, TNT implants tightly attached to the skin tissue (Fig. 10). These results highlight that nanotubular surfaces of titanium achieved greater tissue attachment and less fibrous capsule formation compared to the flat surfaces. Moreover complete soft tissue integration with the implants can form a barrier to invading microorganisms. As a whole, titanium with nanotubular structure can be considered a promising percutaneous implant for orthopedic surgery applications.

5. Conclusions

Titania nanotubes on titanium surfaces exhibited antibacterial activity and anti-infection ability both in vitro and in vivo. Titania nanotubes had better antibacterial activities compared with pure titanium under the visible light, especially the TNT-100 showed 70% antibacterial efficiencies. In vivo, the surfaces with the nanotubes were more favorable for skin integration due to the more proteins adsorption. Nanotubular implants showed less inflammatory cytokines release and excellent tissue attachment compared with pure titanium in the postoperative infection model. The complete integration made a barrier for preventing the microorganism intrusion and decreased the infection risk of the percutaneous implants. Though the titania nanotubes on titanium surfaces were effective in reducing the risk of infection, but the efficient can be further improved.

Acknowledgements

This work was supported by the National Basic Research Program of China (973 Program, 2012CB933600), National Natural Science Foundation of China (51372210) and the Research Fund for the Doctoral Program of Higher Education of China (20130184110023).

References

[1] J. Tillander, K. Hagberg, L. Hagberg, R. Branemark, Osseointegrated titanium implants for limb prostheses attachments: infectious complications, Clin. Orthop. Relat. Res. 468 (10) (2010) 2781–2788.
[2] S. Jeyapalina, J.P. Beck, K.N. Bachus, D.L. Williams, R.D. Bloebaum, Efficacy of a porous-structured titanium subdermal barrier for preventing infection in percutaneous osseointegrated prostheses, J. Orthop. Res. 30 (8) (2012) 1304–1311.
[3] A.F. von Recum, J.B. Park, Permanent percutaneous devices, Crit. Rev. Bioeng. 5 (1981) 37–77.
[4] A. Peramo, C.L. Marcelo, Bioengineering the skin-implant interface: the use of regenerative therapies in implanted devices, Ann. Biomed. Eng. 38 (2010) 2013–2031.
[5] A.F. von Recum, Applications and failure modes of percutaneous devices: a review, J. Biomed. Mater. Res. 18 (4) (1984) 323–336.
[6] G.D. Winter, Transcutaneous implants: reactions of the skin-implant interface, J. Biomed. Mater. Res. 8 (3) (1974) 99–113.
[7] Y. Fukano, M.L. Usui, R.A. Underwood, S. Isenhath, A.J. Marshall, K.D. Hauch, B.D. Ratner, J.E. Olerud, P. Fleckman, Epidermal and dermal integration into sphere-templated porous poly(2-hydroxyethyl methacrylate) implants in mice, J. Biomed. Mater. Res. A 94 (4) (2010) 1172–1186.
[8] M. Lamghari, H. Huet, A. Laurent, S. Berland, E. Lopez, A model for evaluating injectable bone replacements in the vertebrae of sheep: radiological and histological study, Biomaterials 20 (22) (1999) 2107–2114.
[9] J.A. Jansen, J.P. van der Waerden, H.B. van der Lubbe, K. de Groot, Tissue response to percutaneous implants in rabbits, J. Biomed. Mater. Res. 24 (1990) 295–307.
[10] D.G. Kim, S.S. Huja, B.C. Tee, P.E. Larsen, K.S. Kennedy, H.H. Chien, J.W. Lee, H.B. Wen, Bone ingrowth and initial stability of titanium and porous tantalum dental implants: a pilot canine study, Implant Dent. 22 (4) (2013) 399–405.
[11] P. Bonding, Titanium implants for bone-anchored hearing aids-host reaction, Acta Otolaryngol. Suppl. 543 (2000) 105–107.
[12] D.A. Puleo, R.A. Kissling, M.S. Sheu, A technique to immobilize bioactive proteins, including bone morphogenetic protein-4 (BMP-4), on titanium alloy, Biomaterials 23 (2002) 2079–2087.
[13] A. Oyane, K. Hyodo, M. Uchida, Y. Sogo, A. Ito, Preliminary in vivo study of apatite and laminin-apatite composite layers on polymeric percutaneous implants, J. Biomed. Mater. Res. B: Appl. Biomater. 97 (1) (2011) 96–104.

[14] E.L. Perry, J.P. Beck, D.L. Williams, R.D. Bloebaum, Assessing peri-implant tissue infection prevention in a percutaneous model, J. Biomed. Mater. Res. B: Appl. Biomater. 92 (2) (2010) 397–408.
[15] M. Pitkin, J. Pilling, G. Raykhtsaum, Mechanical properties of totally permeable titanium composite pylon for direct skeletal attachment, J. Biomed. Mater. Res. B: Appl. Biomater. 100 (2012) 993–999.
[16] P.A. Federspil, A. Koch, M.H. Schneider, K. Zaoui, Percutaneous titanium implants for bone conduction hearing aids: experience with 283 cases, HNO 62 (July (7)) (2014) 490–497.
[17] X.F. Walboomers, J.A. Jansen, Effect of microtextured surfaces on the performance of percutaneous devices, J. Biomed. Mater. Res. A 74 (3) (2005) 381–387.
[18] H. Kim, H. Murakami, B. Chehroudi, M. Textor, D.M. Brunette, Effects of surface topography on the connective tissue attachment to subcutaneous implants, Int. J. Oral Maxillofac. Implants 21 (3) (2006) 354–365.
[19] C.A. Middleton, C.J. Pendegrass, D. Gordon, J. Jacob, G.W. Blunn, Fibronectin silanized titanium alloy: a bioinductive and durable coating to enhance fibroblast attachment in vitro, J. Biomed. Mater. Res. A 83 (4) (2007) 1032–1038.
[20] D.J. Gordon, D.D. Bhagawati, C.J. Pendegrass, C.A. Middleton, G.W. Blunn, Modification of titanium alloy surfaces for percutaneous implants by covalently attaching laminin, J. Biomed. Mater. Res. A 94 (2) (2010) 586–593.
[21] X. Ge, Y. Leng, C. Bao, S.L. Xu, R. Wang, F. Ren, Antibacterial coatings of fluoridated hydroxyapatite for percutaneous implants, J. Biomed. Mater. Res. A 95 (2) (2010) 588–599.
[22] C.J. Pendegrass, A.E. Goodship, G.W. Blunn, Development of a soft tissue seal around bone-anchored transcutaneous amputation prostheses, Biomaterials 27 (23) (2006) 4183–4191.
[23] B. Chehroudi, D.M. Brunette, Subcutaneous microfabricated surfaces inhibit epithelial recession and promote long-term survival of percutaneous implants, Biomaterials 23 (1) (2002) 229–237.
[24] S.N. Isenhath, Y. Fukano, M.L. Usui, R.A. Underwood, C.A. Irvin, A.J. Marshall, K.D. Hauch, B.D. Ratner, P. Fleckman, J.E. Olerud, A mouse model to evaluate the interface between skin and a percutaneous device, J. Biomed. Mater. Res. A 83 (4) (2007) 915–922.
[25] M. Pitkin, G. Raykhtsaum, J. Pilling, O.V. Galibin, M.V. Protasov, J.V. Chihovskaya, et al., Porous composite prosthetic pylon for integration with skin and bone, J. Rehabil. Res. Dev. 44 (5) (2007) 723–738.
[26] S.D. Puckett, P.P. Lee, D.M. Ciombor, R.K. Aaron, T.J. Webster, Nanotextured titanium surfaces for enhancing skin growth on transcutaneous osseointegrated devices, Acta Biomater. 6 (6) (2010) 2352–2362.
[27] B.J. Farrell, B.I. Prilutsky, J.M. Ritter, S. Kelley, K. Popat, M. Pitkin, Effects of pore size, implantation time, and nano-surface properties on rat skin ingrowth into percutaneous porous titanium implants, J. Biomed. Mater. Res. A 102 (5) (2014) 1305–1315.
[28] H. Bai, Z. Liu, L. Liu, D.D. Sun, Large-scale production of hierarchical TiO_2 nanorod spheres for photocatalytic elimination of contaminants and killing bacteria, Chemistry 19 (9) (2013) 3061–3070.
[29] H.W. Wang, H.R. Cheng, F.Q. Wang, D.Z. Wei, X.D. Wang, An improved 3-(4,5-dimethylthiazol-2-yl)-2,5-diphenyl tetrazolium bromide (MTT) reduction assay for evaluating the viability of *Escherichia coli* cells, J. Microbiol. Methods 82 (2010) 330–333.
[30] L. Yuan, D. Nin, X.Y. Tang, J. Li, Study of the viable count of *Staphylococcus aureus* by MTT assay, J. South-Central Univ. Natl. 33 (2) (2014) 54–56, 84 (in Chinese).
[31] H.R. Li, Q. Cui, B. Feng, J.X. Wang, X. Lu, J. Weng, Antibacterial activity of TiO_2 nanotubes: influence of crystal phase, morphology and Ag deposition, Appl. Surf. Sci. 284 (2013) 179–183.
[32] B.S. Smith, S. Yoriya, T. Johnson, K.C. Popat, Dermal fibroblast and epidermal keratinocyte functionality on titania nanotube arrays, Acta Biomater. 7 (6) (2011) 2686–2696.
[33] A.G. Gristina, Biomaterial-centered infection: microbial adhesion versus tissue integration, Science 237 (1987) 1588–1595.
[34] K.G. Neoh, X. Hu, D. Zheng, E.T. Kang, Balancing osteoblast functions and bacterial adhesion on functionalized titanium surfaces, Biomaterials 33 (10) (2012) 2813–2822.